Direct neutron-diffraction-based measurement of magnetic order in brownmillerite $SrCoO_{2.5}$ and $La_{0.5}Sr_{0.5}CoO_{2.5}$ thin films

Cite as: APL Mater. 12, 041123 (2024); doi: 10.1063/5.0196646
Submitted: 8 January 2024 • Accepted: 1 April 2024 •
Published Online: 18 April 2024 • Publisher Error Corrected: 19 April 2024

William M. Postiglione,[1] Jierui Liang,[1] Nileena Nandakumaran,[1] Lucca Figari,[1] Adam A. Aczel,[2] and Chris Leighton[1,a)]

AFFILIATIONS

[1] Department of Chemical Engineering and Materials Science, University of Minnesota, Minneapolis, Minnesota 55455, USA
[2] Neutron Scattering Division, Oak Ridge National Laboratory, Oak Ridge, Tennessee 37830, USA

[a)] Author to whom correspondence should be addressed: leighton@umn.edu

ABSTRACT

Epitaxial cobaltites have emerged as exemplary materials for electrochemical gating, in large part due to their topotactic perovskite (P) ↔ brownmillerite (BM) transformations. $SrCoO_{3-\delta}$, for example, can be cycled between metallic ferromagnetic P $SrCoO_3$ and insulating BM $SrCoO_{2.5}$, realizing exceptional modulation of electronic, thermal, and optical properties. It is often presumed that such cycling also generates ferromagnetic–antiferromagnetic (F-AF) modulation due to the G-type AF order in *bulk* $SrCoO_{2.5}$. Little is understood about magnetism in *thin-film* BM $SrCoO_{2.5}$, however, meaning that the true magnetic property modulation is unclear. We address this here through a neutron diffraction study of BM $La_{1-x}Sr_xCoO_{2.5}$ films at $x = 0.5$ and 1.0. Lightly compressively strained $SrCoO_{2.5}$ films are shown to retain G-type AF order, albeit with suppressed Néel temperature (~340 K). Of high interest for AF spintronics, room-temperature F–AF cycling is thus possible across the $SrCoO_{3-\delta}$ P ↔ BM transformation. At $x = 0.5$, however, BM $La_{0.5}Sr_{0.5}CoO_{2.5}$ films are found to exhibit no detectable G-type AF order but instead weak F order (Curie temperature ~115 K), unveiling a $La_{0.5}Sr_{0.5}CoO_{3-\delta}$ phase diagram with *two* distinct F phases. These results thus uncover new, unanticipated magnetic phase behavior in these materials, in addition to being directly relevant to cobaltite-based magnetoionics.

INTRODUCTION

Recent advances in the areas of complex oxide films and heterostructures, and particularly their active control, have put a fresh spotlight on brownmillerite (BM) phases.[1–20] These structures, which were previously relatively obscure, can be obtained from perovskite (P) ABO_3 by reduction to $ABO_{3-\delta}$ with large oxygen deficiency δ. Contrasting with the randomly distributed oxygen vacancies (V_O) in P $ABO_{3-\delta}$ compounds, there exists a homologous series of phases at fractional δ (*e.g.*, δ = 0.25, 0.50) with spatially ordered V_O.[21–31] BM phases, which have δ = 0.5, i.e., $ABO_{2.5}$ or $A_2B_2O_5$,[21–31] stand out in terms of stability, to the point that the reduction of ABO_3 films often proceeds directly to BM $ABO_{2.5}$, premier examples being the transformations between P $SrCoO_3$ and BM $SrCoO_{2.5}$[1–14] and between P $SrFeO_3$ and BM $SrFeO_{2.5}$.[9,15–20] Reversible transformation between these phases was first demonstrated thermally, at relatively low reduction and oxidation temperatures.[1,2,6,14,15,18,20] More recently, these transformations have been triggered electrically, at low voltage and power, in a reversible, non-volatile fashion. This has been achieved in electrochemical transistors, using oxygen conductors,[3,10] or electrolytes such as ionic liquids and gels,[4,5,7,9–13,16,19] to enable gate-voltage-controlled redox. Due to the very different properties in P and BM phases, electrochemical gating of materials such as $SrCoO_{3-\delta}$ and $SrFeO_{3-\delta}$ has thus realized extraordinary modulations of electronic, magnetic, optical, and thermal properties, raising prospects for applications in neuromorphic and stochastic computing, magnetoionics, voltage-tunable photonics, thermal management, etc.[3–5,7–13,16,19,32–36]

Taking $SrCoO_{3-\delta}$ as an example, reversible topotactic transformations between cubic P $SrCoO_3$ and orthorhombic BM $SrCoO_{2.5}$ are now well established, both thermally[1,2,6,14] and electrically.[3–5,7–13]

Due to the high ambient-temperature diffusivities of V_O in such cobaltites[21,37–39] and their low energies of formation,[40–42] electrical toggling between P $SrCoO_{3-\delta}$ and BM $SrCoO_{2.5}$ has been achieved at room temperature via ionic liquid/gel gating.[4,5,7,9,10,12,13] The cobaltite P → BM transformation is understood to be first-order[42,43] (proceeding through a regime of P/BM phase coexistence), eventually generating orthorhombic BM with alternating oxygen deficient and sufficient planes along [001], in which V_O organize along [110] directions.[24–28] This creates alternating octahedral and tetrahedral Co–O coordination[24–28] and thus very different physical properties to P $SrCoO_3$ (which has only octahedral Co^{4+}). Fully oxygenated P $SrCoO_3$, while typically unstable at ambient, is a metallic, ferromagnetic (F) oxide with Curie temperature up to $T_C \approx 305$ K.[44–46] Meanwhile, BM $SrCoO_{2.5}$ is insulating, transparent, and non-F,[21,26,27,30,47–49] meaning that reversible, non-volatile toggling between P and BM phases realizes wide modulations of electronic, optical, and thermal properties.[1–8,10,11]

The extent and nature of the modulation of *magnetic* properties, however, which are the focus of this paper, are less clear. This is because, while *bulk* BM $SrCoO_{2.5}$ is known to exhibit antiferromagnetic (AF) order,[26,27,30,47,48] the magnetism in *thin-film* $SrCoO_{2.5}$[1,2,4,5,7,8,11–13,50,51] is not well understood. Bulk $SrCoO_{2.5}$ is a G-type AF with a high Néel temperature (T_N) of 540–570 K,[27,47,48] as determined by neutron powder diffraction.[26,27,47,48] Neutron diffraction is a direct but signal-limited probe and is thus challenging to apply to thin-film BM $SrCoO_{2.5}$. Consequently, the literature on magnetism in $SrCoO_{2.5}$ films is rather unclear. G-type AF order with T_N up to 325 K has been reported from neutron diffraction on tensile-strained $DyScO_3/SrCoO_{3-\delta}$ films but was associated with P $SrCoO_{3-\delta}$, not BM $SrCoO_{2.5}$.[52] Compressive $SrTiO_3/SrCoO_{2.5}$ films have been studied by spectroscopy [including x-ray magnetic circular dichroism (XMCD)] and magnetometry, leading to a claim of F order with $T_C > 300$ K.[51] This is in contrast to multiple other XMCD-based reports, however, where no significant F signals were found in BM $SrCoO_{2.5}$, under various strains.[1,4,13] BM $SrCoO_{2.5}$ films, in some cases controlled by electrochemical gating,[5,12] have also been observed to induce exchange bias in adjacent $La_{1-x}Sr_xMnO_3$ and P $SrCoO_{3-\delta}$ layers,[5,12,50] taken as evidence of AF order in BM $SrCoO_{2.5}$ films.[5,12,50] Both AF and F orders have thus been claimed in BM $SrCoO_{2.5}$, with widely varying T_N and T_C. In $SrCoO_{3-\delta}$-based electrochemical transistors, it is therefore well established that the P $SrCoO_3$ phase is F,[1,2,4,5,7,8,11,13] but the nature of the magnetism in the BM $SrCoO_{2.5}$ is not settled,[1,2,4,5,7,8,11–13,50,51] meaning that the true modulation of magnetic properties remains unclear. This is despite the fact that bulk-like magnetic properties in the BM $SrCoO_{2.5}$ state (*i.e.*, AF order with $T_N > 300$ K) would be of exceptional interest in terms of room-temperature F/AF modulation, *e.g.*, to merge magnetoionics[33–36] and AF spintronics.[53,54]

Due to advantages in terms of the stability of the P and BM phases, and additional doping tunability, the $La_{1-x}Sr_xCoO_{3-\delta}$ system is also of interest for thermal,[55–58] getter-induced,[59,60] and electrochemical redox.[42,61–65] Voltage-induced P → BM transformations have recently been demonstrated over almost the entire x range in ion-gel-gated $La_{1-x}Sr_xCoO_{3-\delta}$, with doping- and strain-tunable threshold voltages.[42] This generates an exceptional gate modulation of optical properties in the infrared,[64] as well as of room-temperature electronic and thermal conductivity,[63] of interest for voltage-tuned photonics, thermal transistors, etc. Ionically gated $La_{1-x}Sr_xCoO_{3-\delta}$ films have also been used in studies of reversibility and hysteresis across the P ↔ BM transformation,[43] as well as for optimization of P ↔ BM switching time.[65] Again, however, the true extent of the *magnetic* modulation across such transformations is unclear due to a poor understanding of the magnetism in the BM state. The situation is worse than in $SrCoO_{3-\delta}$, as even in bulk, there is no complete study of magnetic properties of BM $La_{1-x}Sr_xCoO_{2.5}$ as a function of x. A report does exist on bulk $La_{0.33}Sr_{0.67}CoO_{3-\delta}$ studied vs δ via x-ray and neutron diffraction, magnetometry, and transport.[66] As in related cobaltites, multiple phases were observed vs δ, generating a complex evolution of magnetic properties.[66] Weak F order coexisting with AF order was suggested in the BM phase ($\delta \approx 0.5$), but without a direct probe of the AF ordering.[66] There also exists an intriguing recent study of thermally reduced $La_{0.7}Sr_{0.3}CoO_{3-\delta}$ films.[56] In the BM phase, that work found no evidence of magnetic order from magnetometry, but weak F order in XMCD, and potential AF order in x-ray linear dichroism.[56] As in $SrCoO_{3-\delta}$, the P phase of $La_{1-x}Sr_xCoO_{3-\delta}$ is thus well understood magnetically,[1,2,4,5,7,8,11,13,42,43,56,61,65] while the BM phase remains poorly understood, especially in films, meaning that the true modulation of magnetic properties by thermal or electrochemical redox is unknown.

In light of the above, here we provide the first detailed study of the structure and magnetism of epitaxial BM $La_{1-x}Sr_xCoO_{2.5}$ films, using high-resolution x-ray diffraction (HRXRD), neutron diffraction, and magnetometry, augmented with complementary bulk measurements, focused on $x = 1.0$ and 0.5. $SrCoO_{2.5}$(001) films were directly deposited on LSAT $[(LaAlO_3)_{0.3}(SrTaAlO_6)_{0.7}]$ substrates, while LSAT/$La_{0.5}Sr_{0.5}CoO_{3-\delta}$(001) films were deposited in the P phase and then gradually reduced to BM. Neutron diffraction experiments on LSAT/$SrCoO_{2.5}$(50 nm) films detect a magnetic-only (201) reflection, directly confirming bulk-like G-type AF order, albeit with reduced $T_N \approx 340$ K. No such peak is detected in LSAT/$La_{0.5}Sr_{0.5}CoO_{2.5}$(200 nm) films, however, which instead reveal F order with $T_C \approx 115$ K, but with saturation magnetization only ~0.1 μ_B/Co. $SrCoO_{3-\delta}$ films are thus confirmed to enable toggling between room-temperature F and AF states, while $La_{0.5}Sr_{0.5}CoO_{3-\delta}$ films enable switching between conventional F and weak F states. The structural and magnetic phase diagrams of thin-film $La_{0.5}Sr_{0.5}CoO_{3-\delta}$ are then presented as a function of δ, elucidating the transformation between the P F and reentrant BM F phases. These results thus uncover new, unanticipated magnetic phase behavior in these materials, in addition to being directly relevant to cobaltite-based magnetoionics.

METHODS

$x = 1$ BM $SrCoO_{2.5}$ films were directly deposited, while $x = 0.5$ films were deposited in the P phase and then reduced to BM $La_{0.5}Sr_{0.5}CoO_{2.5}$. High-pressure-oxygen sputtering was employed, on LSAT(001) substrates, generating approximately −0.9% and −0.3% lattice mismatches for $x = 1$ and 0.5 BM films, respectively (see Table S1 of the supplementary material for details). P $La_{0.5}Sr_{0.5}CoO_{3-\delta}$ was deposited from a P $La_{0.5}Sr_{0.5}CoO_3$ target,[42,43,61,63,64,67] while BM $SrCoO_{2.5}$ was deposited from a mixed-phase Sr–Co–O target with a 1:1 Sr/Co ratio. The substrates were

pre-annealed in 1 Torr of O_2 at 900 °C for 15–30 min. The growth conditions included temperatures of 600 °C (for x = 0.5 films), 700–750 °C (for x = 1 films), 50–70 W DC powers, and 1.5 Torr flowing O_2 (99.999%). Post-deposition cooling was done in 1.5 Torr of O_2 for x = 1 BM $SrCoO_{2.5}$ and 600 Torr of O_2 for x = 0.5 P LSCO. 50-nm-thick $SrCoO_{2.5}$ and 100–200-nm-thick $La_{0.5}Sr_{0.5}CoO_{2.5}$ films were studied, as determined by grazing incidence x-ray reflectivity and/or wide-angle HRXRD (via Laue fringes). The BM $SrCoO_{2.5}$ films were limited to 50 nm by chemical phase separation above this thickness, into $Sr_6Co_5O_{15}$, Co_3O_4, and a non-BM $SrCoO_{3-\delta}$ phase, potentially linked to strain relaxation. The thermal reduction of P $La_{0.5}Sr_{0.5}CoO_{3-\delta}$ films was achieved by vacuum ($<1 \times 10^{-7}$ Torr) post-annealing, at ≥500 °C. This was done via sequential 4-hr anneals at progressively higher temperatures, performing HRXRD and magnetometry after each anneal; this resulted in near-phase-pure BM by ~540 °C.

HRXRD was performed in a Rigaku SmartLab XE with Cu $K_{\alpha 1}$ radiation (λ = 1.5406 Å). Thin-film magnetometry employed a Quantum Design PPMS vibrating sample magnetometer (VSM) and/or a Quantum Design MPMS-3 SQUID VSM from 10 to 300 K in applied magnetic fields to 70 kOe. Neutron diffraction was performed on the VERITAS (HB-1A) beamline of the High-Flux Isotope Reactor, Oak Ridge National Laboratory, at λ = 2.37 Å. For x = 1 BM $SrCoO_{2.5}$ films, neutron diffraction was done on a stack of six 50-nm-thick films, on 20 × 20 mm^2 LSAT(001) substrates. For x = 0.5 BM $La_{0.5}Sr_{0.5}CoO_{2.5}$ films, a single 200-nm-thick film was used [also on 20 × 20 mm^2 LSAT(001)]. Large substrates, relatively thick films, and stacking (as necessary) were used to maximize the diffracted intensity. The samples were wired to thin Al plates, with the film (*h0l*) scattering plane horizontal, and loaded into a closed cycle refrigerator operating between 3.5 and 750 K (in He exchange gas below 300 K). A collimator configuration of 40′–40′–40′–80′ yielded an energy resolution [full width at half maximum (FWHM)] of ~1 meV at the elastic line. The combination of a double-bounce monochromator and the placement of the pyrolytic graphite crystal analyzer for energy discrimination before the single He-3 detector provided excellent signal-to-noise, as needed for thin-film magnetic diffraction. Higher-order wavelength contamination of the incident beam was minimized through two pyrolytic graphite filters.

Reference bulk samples of BM $SrCoO_{2.5}$ and $La_{0.5}Sr_{0.5}CoO_{2.5}$ were also prepared by standard ceramic routes. Stoichiometric mixtures of La_2O_3, $SrCO_3$, and Co_3O_4 were first ground and reacted multiple times at 1000 °C. Powders were then cold-pressed and sintered for 24 h at 1200 °C in O_2 or 1100 °C in air, for x = 0.5 and x = 1, respectively. To reach phase-pure BM, resulting x = 0.5 P $La_{0.5}Sr_{0.5}CoO_{3-\delta}$ pellets were powdered and then reduced at 250 °C in flowing forming gas (95% N_2/5% H_2).[68] To the same end, x = 1 pellets were quenched in liquid N_2 from ~1000 °C after sintering.[27] Powder x-ray diffraction (PXRD) in a Rigaku MiniFlex (Cu K_α radiation) was used to confirm the BM phase in both cases. Bulk magnetometry employed a Quantum Design PPMS VSM, a Quantum Design MPMS-3 SQUID VSM, or an 8600 series Lakeshore VSM, between 10 and 600 K in fields to 1 kOe. Differential scanning calorimetry (DSC) was performed using a TA Instruments Q1000 calorimeter from 90 to 573 K.

RESULTS AND ANALYSIS

Figure 1 shows the HRXRD structural characterization of LSAT/$SrCoO_{2.5}$(50 nm) and LSAT/$La_{0.5}Sr_{0.5}CoO_{3-\delta}$(100 nm) films. The lower (black) curve in Fig. 1(a) shows a wide-range specular HRXRD scan from an LSAT/$SrCoO_{2.5}$ film grown under optimized conditions for BM formation (see Methods). Aside from the substrate peaks, only $SrCoO_{2.5}$ BM reflections are found, spanning (002) through (00$\underline{12}$), clearly confirming phase-pure BM with the expected unit-cell quadrupling relative to P $SrCoO_{3-\delta}$.[21,22,24–27] As shown in Fig. 1(b), which is color-coordinated with Fig. 1(a), the FWHM of the BM 008 rocking curve is ~0.08°; while larger than the equivalents in P $La_{1-x}Sr_xCoO_{3-\delta}$ films,[42,43,61,63,64,67] this is respectable, pointing to high epitaxial quality. The remainder of the curves in Fig. 1(a) (colored) are for LSAT/$La_{0.5}Sr_{0.5}CoO_{3-\delta}$, from the as-deposited case (top) to the 540 °C vacuum annealed case (bottom). A clear evolution is evident, from phase-pure P as deposited [only (001), (002), (003) P peaks] to near-phase-pure BM after 540 °C annealing [dominant BM (002) to (00$\underline{12}$) peaks]. We use the term "near-phase-pure" here, as a very minor, broad peak does arise near 43°, potentially indicating a very low volume fraction of CoO nanoregions. As shown in Fig. 1(b), the P (002) rocking curve widths are lower in these x = 0.5 films, lying at ~0.04°. Nevertheless, all the rocking curve widths in Fig. 1(b) are broadened with respect to typical values for the LSAT substrates (~0.01°), indicating some additional disorder in BM films of this thickness relative to the substrates, and to equivalent P films. The asymmetric [P (103)/BM (11$\underline{12}$)] reciprocal space maps in Figs. 1(c) and 1(d) further illustrate that these $La_{0.5}Sr_{0.5}CoO_{3-\delta}$ films are fully strained to the LSAT substrates, even at this 100 nm thickness. The film and substrate reflections clearly occur at the same h, with no indication of relaxation toward the bulk positions (black/white "X" marks) in the BM [Fig. 1(d)], or particularly the P phase [Fig. 1(c)]. At the 200 nm thickness used for neutron diffraction experiments (see below), very similar reciprocal space maps and lattice parameters were found, confirming fully strained films at that thickness also.

Further detail on the vacuum-annealing-induced transformation from P to BM in LSAT/$La_{0.5}Sr_{0.5}CoO_{3-\delta}$ films is provided in the close-up around the P (002)/BM (008) region in Fig. 1(e). The as-deposited P (002) peak (purple) can now be seen to be flanked by Laue fringes, further evidencing high epitaxial quality, particularly low interface/surface roughness. Annealing at 500 °C results in the blue curve in Fig. 1(e), with a distinctly downshifted P (002) peak, revealing significant V_O formation.[42,61] This peak also exhibits slight asymmetry, indicating distinct regions with different out-of-plane lattice parameters. After 520 °C annealing (gold curve), the situation changes significantly; two clearly distinct peaks now arise, both to the left of the LSAT (002) reflection. One lies at the BM (008) position and is relatively sharp, while the other lies between P (002) and BM (008) and is obviously broadened. The latter peak, in fact, lies close to the position expected of a tetragonal $La_{1-x}Sr_xCoO_{2.75}$ phase previously detected in bulk x = 0.67 samples (as do small peaks in some of the other curves near 46.1°).[66] Such phases with δ intermediate between P and BM are well known in bulk $La_{1-x}Sr_xCo(Fe)O_{3-\delta}$ but rarely observed in films, aside from in local regions.[20,69,70] In the 520 °C case in Fig. 1(e), the peak at the BM (008) location has a width almost commensurate with the total film thickness, meaning that the phase separation into regions with distinct δ must occur laterally not

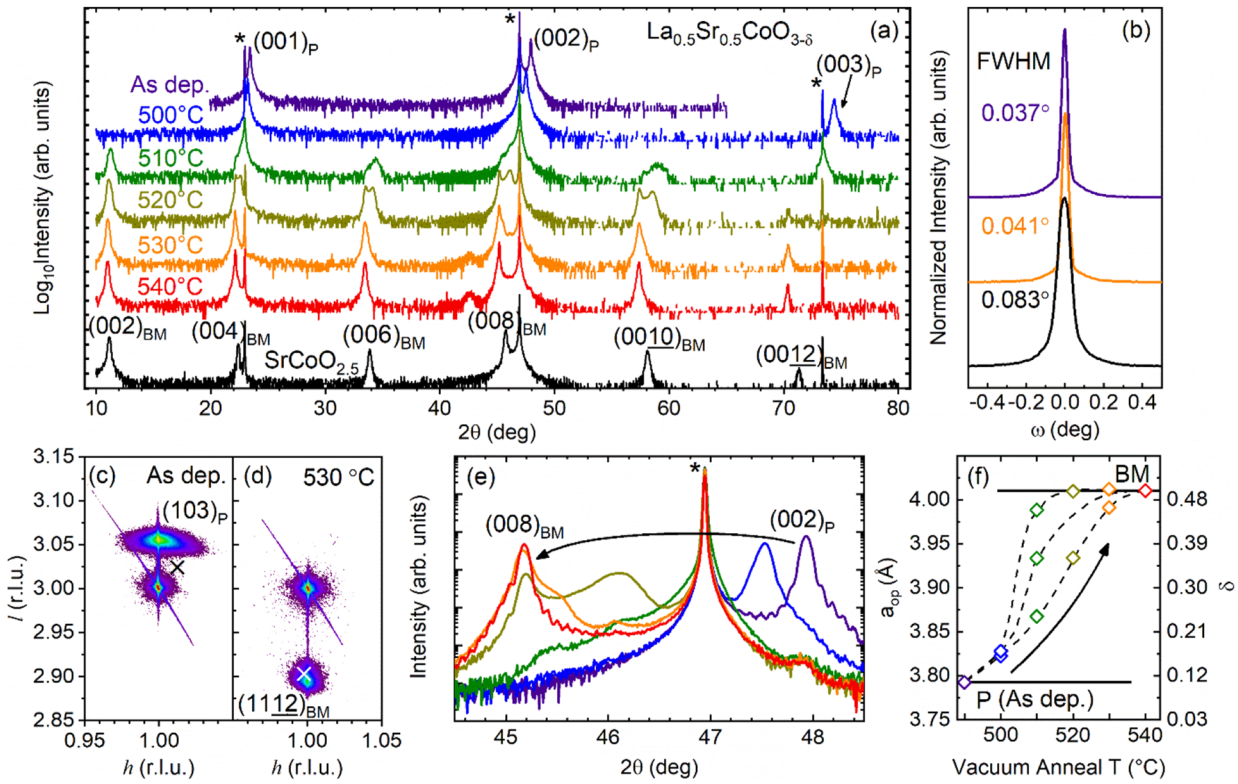

FIG. 1. High-resolution x-ray diffraction characterization of epitaxial brownmillerite $La_{1-x}Sr_xCoO_{2.5}$ thin films. (a) Wide-range high-resolution specular x-ray diffraction scans (intensity vs 2θ) from an as-deposited LSAT/$SrCoO_{2.5}$(50 nm) film (black, bottom) and LSAT/$La_{0.5}Sr_{0.5}CoO_{3-\delta}$(100 nm) films in the as-deposited state and at various shown reduction temperatures (colored data, vertically shifted for clarity). The subscript "P" refers to perovskite, and all other reflections are brownmillerite (BM). The asterisks label substrate (LSAT) reflections. (b) P (002)/BM (008) rocking curves for selected films from (a) [color coded as in (a)], with the respective full width at half maximum (FWHM) values shown. (c) and (d) Representative asymmetric reciprocal space maps around the $(103)_P$ and $(11\bar{2}12)_{BM}$ reflections of an as-deposited $La_{0.5}Sr_{0.5}CoO_{3-\delta}$ P film (c) and a 530 °C-reduced $La_{0.5}Sr_{0.5}CoO_{3-\delta}$ BM film (d). *h* and *l* are in substrate reciprocal lattice units, and the black/white crosses mark the expected bulk positions. (e) Close-up of the high-resolution specular x-ray diffraction scans on $La_{0.5}Sr_{0.5}CoO_{3-\delta}$ films from (a) [color coded as in (a)]. (f) Vacuum annealing temperature dependence of the out-of-plane pseudocubic lattice parameter of $La_{0.5}Sr_{0.5}CoO_{3-\delta}$ films [color coded as in (a)]. The as-deposited film is shown at 490 °C. The phase-pure P and BM states are marked by horizontal solid lines. The dashed lines are guides to the eye, and multiple points at a given temperature indicate multiple distinct peaks in (e). The right axis shows an estimated conversion to average oxygen deficiency δ based on linear interpolation between the P and BM states (see Fig. S1 of the supplementary material).[19,42,43,67]

through the depth; slight thermal gradients during annealing could play a role in this. At 530 °C (orange curve), the BM (008) peak then becomes dominant, by 540 °C (red curve) reaching a situation where a single, symmetric BM (008) peak with abundant Laue fringes is found. Near-phase-pure, high-quality BM $La_{0.5}Sr_{0.5}CoO_{2.5}$ is thus evidenced after 540 °C vacuum annealing of LSAT/$La_{0.5}Sr_{0.5}CoO_{3-\delta}$ films.

The evolution with annealing temperature is shown in Fig. 1(f), where the P and BM states are marked with horizontal solid black lines, and cases with multiple peaks in Fig. 1(e) are plotted as distinct out-of-plane lattice parameters (a_{op}). Note that BM points here are divided by 4 (due to the unit cell quadrupling[21–27,31,66,68]) to facilitate easy comparisons. The overall pseudocubic cell volume expansion is clear,[42,43,61] as is the progression through intermediate states with distinct lattice parameters, ultimately leading to essentially phase-pure BM at 540 °C. Based on established linear interpolation between the lattice parameters of the P and BM states of $La_{0.5}Sr_{0.5}CoO_3$ and $La_{0.5}Sr_{0.5}CoO_{2.5}$,[42] the right axis shows a conversion to approximate δ (see Fig. S1 of the supplementary material for more details). The as-deposited P LSAT/$La_{0.5}Sr_{0.5}CoO_{3-\delta}$ films have a slightly expanded lattice parameter due to non-zero δ, as expected,[42] while the BM LSAT/$La_{0.5}Sr_{0.5}CoO_{3-\delta}$ after full thermal reduction has δ very close to that expected of BM $La_{0.5}Sr_{0.5}CoO_{2.5}$.[42]

We now turn to neutron diffraction measurements on these films, the primary goal of this work, starting with BM $SrCoO_{2.5}$. In terms of searching for bulk-like AF order in such films, as shown in Table I, there exist a number of magnetic-only reflections in G-type AF BM $SrCoO_{3-\delta}$.[27] In LSAT/$SrCoO_{2.5}$ films, however, a significant number of these, including some of the highest magnetic structure factor peaks (Table I), overlap with peaks from the LSAT substrate (or the Al sample holder). Many of these substrate peaks are nominally forbidden in the LSAT space group ($Pm\bar{3}m$[71]) but were nevertheless found, at significant intensities. In fact, only

TABLE I. Details of magnetic-only neutron diffraction peaks in the (*h*0*l*) plane for G-type antiferromagnetic $SrCoO_{2.5}$ and potential obscuring features in thin films on LSAT substrates. *Q* and *F* designate the scattering wave vector magnitude and calculated neutron magnetic structure factor, respectively. These data identify the 201 reflection (highlighted) as ideal.

h	*k*	*l*	*Q* (Å^{-1})	F^2	Obscuring peaks
1	0	2	1.3860	14.382	Substrate (0.5, 0.5, 0.5)
1	0	6	2.6622	8.804	Substrate (0.5, 0.5, 1.5)
1	0	10	4.1737	3.564	Substrate (0.5, 0.5, 2.5)
3	0	2	3.4815	3.189	Substrate (1.5, 1.5, 0.5)
3	0	6	4.1578	2.052	Substrate (0.5, 0.5, 2.5)
2	0	1	2.2939	1.237	None
2	0	3	2.5599	1.097	Al powder ring ($q \approx 2.7$)

the (201) reflection expected in G-type AF BM $SrCoO_{2.5}$[27] lies at a scattering wave vector (*Q*) devoid of substrate interference. This peak was therefore selected for initial experimentation, despite its smaller magnetic structure factor than some other magnetic peaks. The (201) plane is superimposed on the bulk G-type AF spin structure[27] in the LSAT/$SrCoO_{2.5}$ schematic in Fig. 2(a). Figure 2(b) shows a background-subtracted 3.5-K rocking curve through the (201) region of the sixfold-stacked LSAT/$SrCoO_{2.5}$(50 nm) sample described in Methods. Notably, a clear peak is present, and, as shown in the background-subtracted 2θ scans in Fig. 2(c), this peak is strongly temperature (*T*) dependent, the scattering essentially vanishing by 350 K. The expected location for the magnetic-only (201) peak and the strong *T* dependence confirm the magnetic nature of this peak. The integrated peak intensity is shown in Fig. 2(d), revealing a good fit to a mean-field order parameter (with a 3D Ising exponent), yielding $T_N \approx 340$ K. This is significantly lower than the bulk value for BM $SrCoO_{2.5}$,[27,47,48] as confirmed in Fig. 2(e), which shows *T*-dependent magnetic susceptibility and DSC data on bulk BM $SrCoO_{2.5}$ polycrystals. The DSC peak and susceptibility anomaly are similar to prior reports on bulk BM $SrCoO_{2.5}$,[27] suggesting a consistent $T_N \approx 540$ K, in the range of previously reported values (540–570 K[27,47,48]).

The results in Fig. 2 are significant in and of themselves. As described in the Introduction, prior literature on the nature of the magnetism in BM $SrCoO_{2.5}$ films[1,2,4,5,7,8,11–13,50,51] is quite scattered and conflicting, and this is the first direct detection of G-type AF order in BM $SrCoO_{2.5}$ films by neutron diffraction, confirming bulk-like AF order, in contrast to some claims.[51] What is striking, however, is the suppression of T_N from 540 to 570 K in bulk[27,47,48] to 340 K in LSAT/$SrCoO_{2.5}$(50 nm) films. There are several factors that could play a role in this difference, including finite-size effects and dimensional confinement, the film strain state (−0.9% here), and the intertwined factors of the exact δ, the level of perfection of the BM order, and the density of associated V_O defects. It is likely that future work could establish which of these factors

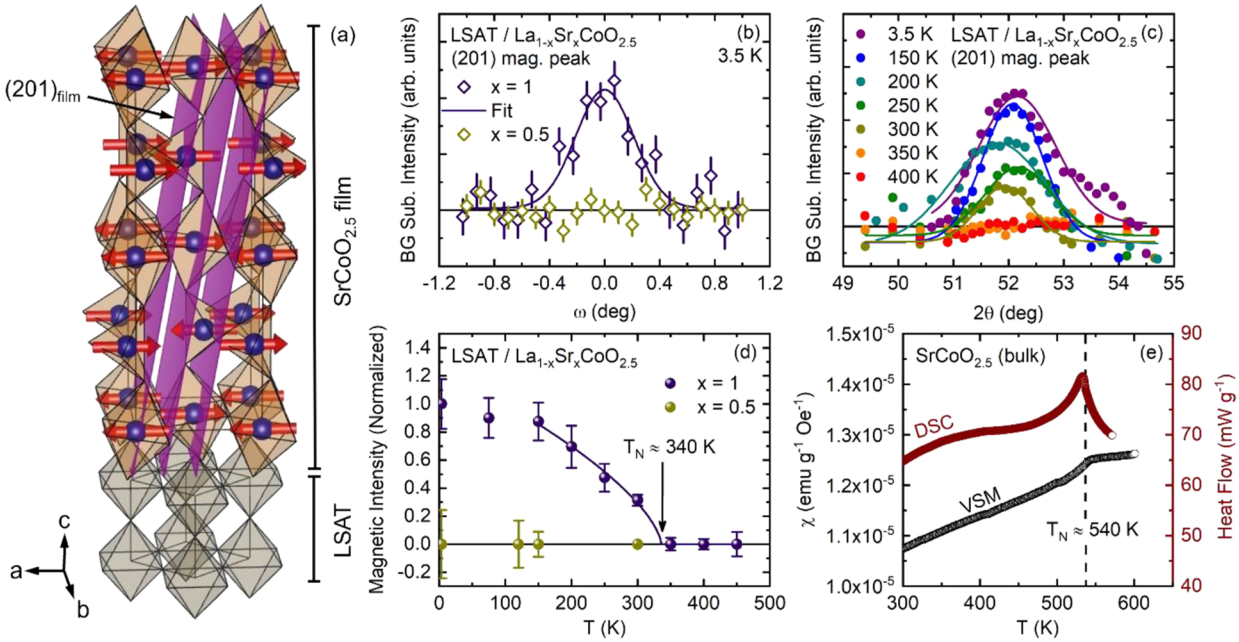

FIG. 2. Probing antiferromagnetic order in epitaxial brownmillerite $SrCoO_{2.5}$ thin films *via* neutron diffraction. (a) LSAT/$SrCoO_{2.5}$ schematic showing the Co ions (blue), Co–O polyhedra (brown), spin orientations in the G-type antiferromagnetic phase (red arrows), and (201) film plane. (b) 3.5-K neutron diffraction 201 rocking curves (background-subtracted intensity vs ω) for brownmillerite $La_{1-x}Sr_xCoO_{2.5}$ films with $x = 1$ (six 50-nm-thick films) and 0.5 (one 200-nm-thick film), with Gaussian fits. (c) Temperature-dependent neutron diffraction 201 scans (background-subtracted intensity vs 2θ) for an $x = 1$ ($SrCoO_{2.5}$) brownmillerite film, with Gaussian fits. (d) Temperature (*T*) dependence of the neutron diffraction intensity (integrated and normalized) of the magnetic (201) peak for $x = 1$ and 0.5 brownmillerite $La_{1-x}Sr_xCoO_{2.5}$ films. The Néel temperature (T_N) is labeled in the $x = 1$ case, and the solid line is a mean-field fit with the 3D Ising exponent. (e) *T* dependence of the magnetic susceptibility (black, left axis) and differential scanning calorimetry heat flow (maroon, right axis) of *bulk* $x = 1$ $SrCoO_{2.5}$; T_N is labeled. The error bars in (b) and (d) derive from standard errors on counts.

is dominant, but it will require a full study of thin-film $SrCoO_{2.5}$ as a function of both compressive and tensile strain through heteroepitaxy on a variety of substrates, coupled with T-dependent neutron diffraction. Such a study would clearly be worthwhile. Our results in Fig. 2 also open the door to future gate-voltage-dependent neutron diffraction measurements in (laterally large) electrochemical transistors.[61,67] Of particular note in this context is that the T_N determined here remains above room temperature, meaning that electrochemical gating could achieve ambient-temperature manipulation of AF order. This is of high interest for AF spintronics, and in terms of connecting the fields of magnetoionics[33–36] and AF spintronics.[53,54]

Given the above findings, similar (201) diffraction peak measurements were also made on LSAT/$La_{0.5}Sr_{0.5}CoO_{2.5}$(200 nm) films in the BM state (after vacuum annealing at 550 °C). As shown in Fig. 2(b), despite the similar total thickness, such x = 0.5 films displayed no detectable 3.5-K intensity in the (201) peak region, nor, in fact, at any T [Fig. 2(d)]. There is thus no detectable G-type AF order in these $La_{0.5}Sr_{0.5}CoO_{2.5}$ films, in contrast with the $SrCoO_{2.5}$ case. Remarkably, however, strongly T-dependent neutron diffraction intensity *was* detected at another Q, specifically the BM (002) peak shown in Fig. 3(b) and in the LSAT/$La_{0.5}Sr_{0.5}CoO_{2.5}$ schematic in Fig. 3(a). The intensity of this peak has negligible T dependence from 300 K down to 100 K, below which it rises significantly. This is illustrated in the integrated peak intensity vs T behavior in Fig. 3(c), which is well fit by a mean-field order parameter (3D Ising exponent), yielding a critical temperature of ~100 K. This indicates the existence of an F component to the magnetic order in LSAT/$La_{0.5}Sr_{0.5}CoO_{2.5}$ with a Curie temperature (T_C) of ~100 K, which, as also shown in Fig. 3(c), does not arise in LSAT/$SrCoO_{2.5}$ films. Unexpectedly, these BM $La_{0.5}Sr_{0.5}CoO_{2.5}$ films thus exhibit an F component [Figs. 3(b) and 3(c)] in the absence of G-type AF order [Figs. 2(b)–2(d)], in contrast to the bulk-like G-type AF order with no F component in BM $SrCoO_{2.5}$ films.

The F behavior is further verified by the T-dependent magnetization response in Fig. 3(d), which evidences F order with $T_C \approx 115$ K in LSAT/$La_{0.5}Sr_{0.5}CoO_{2.5}$, in reasonable agreement with the neutron diffraction data in Fig. 3(c). Notably, complementary measurements on *bulk* BM $La_{0.5}Sr_{0.5}CoO_{2.5}$ also reveal an F behavior, and its absence in the BM $SrCoO_{2.5}$ case, as also shown in Fig. 3(d) (PXRD confirmation of the BM structure of the bulk samples is provided in Fig. S2 of the supplementary material). Magnetization measurements on both film and bulk samples are thus in agreement on the existence of an F component in $La_{0.5}Sr_{0.5}CoO_{2.5}$ that is not present in $SrCoO_{2.5}$ [Fig. 3(d)], entirely consistent with neutron diffraction data [Fig. 3(c)]. The 15-K magnetization vs field plots in Fig. 3(e) further confirm the absence of F magnetization in LSAT/$SrCoO_{2.5}$, as well as its presence in LSAT/$La_{0.5}Sr_{0.5}CoO_{2.5}$ films. The latter exhibit strikingly wide, square hysteresis loops, the coercivity (H_c) reaching ~46 kOe at 15 K and even exceeding the maximum available field at the lowest probed T. Such coercivities are surprising at first sight but are likely simply a consequence of the low saturation magnetization (M_s) of ~0.1 μ_B/Co

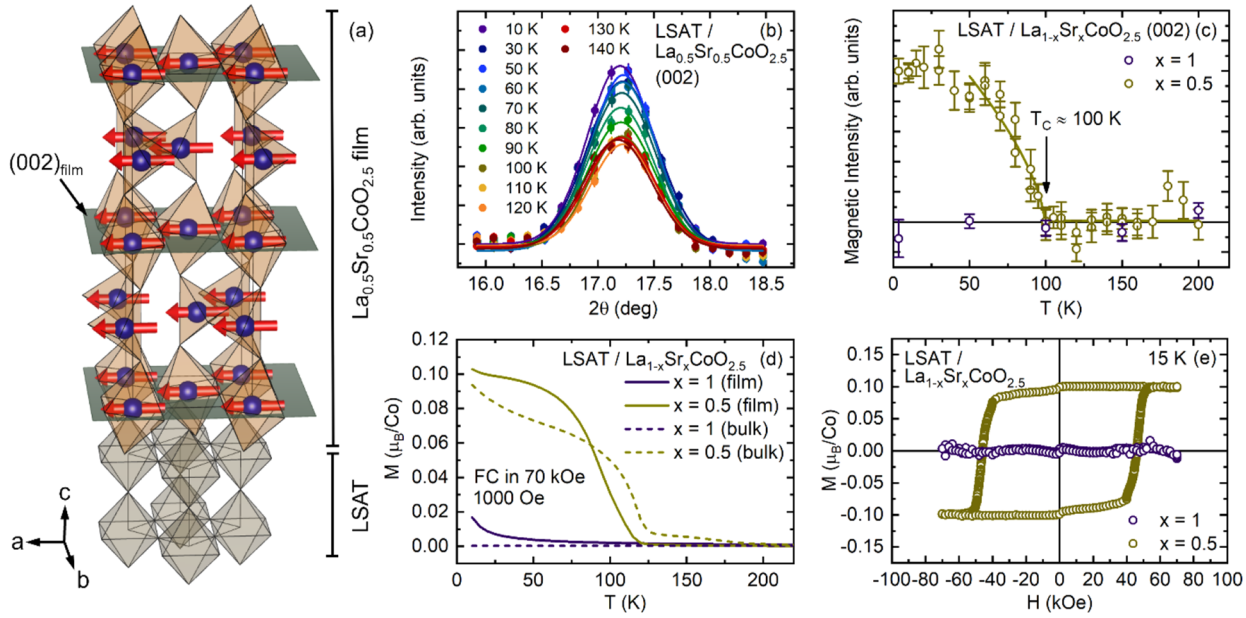

FIG. 3. Probing weak ferromagnetic order in epitaxial brownmillerite $La_{0.5}Sr_{0.5}CoO_{2.5}$ thin films *via* neutron diffraction and magnetometry. (a) LSAT/$La_{0.5}Sr_{0.5}CoO_{2.5}$ schematic showing the Co ions (blue), Co–O polyhedra (brown), spin orientations in the ferromagnetic phase (red arrows), and (002) film plane. (b) Temperature-dependent neutron diffraction 002 scans (intensity vs 2θ) for a 200-nm-thick brownmillerite $La_{0.5}Sr_{0.5}CoO_{2.5}$ film, with Gaussian fits. (c) Temperature (T) dependence of the magnetic 002 neutron diffraction intensity for x = 1 and 0.5 brownmillerite $La_{1-x}Sr_xCoO_{2.5}$ films; the solid line is a mean-field fit with the 3D Ising exponent. (d) T dependence of the magnetization (M) (in 1000 Oe after field cooling in 70 kOe) of x = 1 and 0.5 brownmillerite $La_{1-x}Sr_xCoO_{2.5}$ in bulk (dashed lines) and thin-film (solid lines) forms. (e) 15-K magnetic field (H) dependence of M for x = 1 and 0.5 brownmillerite $La_{1-x}Sr_xCoO_{2.5}$ films. The error bars in (b) and (c) derive from standard errors on counts.

[see Fig. 3(e)]. In the Stoner–Wohlfarth model, for example, $H_c = 2K_u/M_s$, where K_u is the effective uniaxial magnetic anisotropy.[72] While this Stoner–Wohlfarth coercivity represents the maximum H_c in the limit of pure coherent rotation,[72] a weak F behavior with low M_s can thus be seen to naturally support large H_c, as is observed in other weak F systems[73,74] and at magnetization compensation points in ferrimagnets.[75,76]

As noted in the Introduction, there is little understanding of the magnetism in BM $La_{1-x}Sr_xCoO_{2.5}$. A bulk study at $x = 0.67$ *suggested* AF order in the BM phase with a weak F component (notably with similar T_C to our findings),[66] while a thin-film study at $x = 0.33$ detected a weak F signal in XMCD but with an equivocal result on accompanying AF order from x-ray linear dichroism.[56] The new data presented here, including direct neutron diffraction observations, now establish a low-M_s F behavior in BM $La_{0.5}Sr_{0.5}CoO_{2.5}$ unambiguously, but with no evidence for accompanying G-type AF order. While weak ferromagnetism associated with some other type of AF order (*e.g.*, through spin canting[72,74,75]) could only be ruled out by a more comprehensive neutron diffraction study over a wider Q range, the simplest interpretation of our data is a low-M_s pure F state, which the data of Fig. 3(d) suggest exists in both bulk and film BM $La_{0.5}Sr_{0.5}CoO_{2.5}$, with similar T_C. We note that such low-M_s F states are not without precedent in BM-related cobaltites. Zhang *et al.*, for example, recently reported a highly distorted epitaxially stabilized $LaCoO_{2.5}$ phase that exhibits ferromagnetism with T_C approaching ambient but with M_s of only ~0.25 μ_B/Co.[57] In addition, first-principles theoretical work by Zhang and Galli predicts the formation of a metallic weak F state at the interface of P and BM phases in the $La_{1-x}Sr_xCoO_{3-\delta}$ system due to charge transfer.[77]

Further insight into the nature of the weak F state in BM $La_{0.5}Sr_{0.5}CoO_{2.5}$ was obtained through a complete study of LSAT/$La_{0.5}Sr_{0.5}CoO_{3-\delta}$ films vs vacuum-annealing-induced δ. Figure 4(a) first uses the progression shown in Figs. 1(a)–1(e), and 1(f) to estimate the phase fraction of P and BM phases as a function of δ. This phase fraction was estimated by comparing the HRXRD peak intensities of the respective phases (see Fig. S3 of the supplementary material), while the average δ was estimated as described in connection with Figs. 1(f) and S1.[19,42,43,67] The result is shown in Fig. 4(a), which reveals a smooth progression from phase-pure P at oxygen stoichiometries near 3.0 to essentially phase-pure BM at oxygen stoichiometries near 2.5, the implicit variable being the vacuum annealing temperature. This thermally driven topotactic P → BM transformation progresses through a broad P/BM mixed-phase region, as already noted in $La_{1-x}Sr_xCoO_{3-\delta}$-based electrochemical devices, consistent with the first-order nature of the transformation.[42,43] Figures 4(b) and 4(c) then show the accompanying progression in the magnetic properties of these LSAT/$La_{0.5}Sr_{0.5}CoO_{3-\delta}$ films. As expected, at low δ, deep in the P phase, a strong F behavior is observed, with $T_C \approx 240$ K, $M_s \approx 1.5$ μ_B/Co, and 10-K $H_c \approx 0.8$ kOe, typical of thick $La_{0.5}Sr_{0.5}CoO_3$ films.[78] As δ is increased to 0.15 (blue),

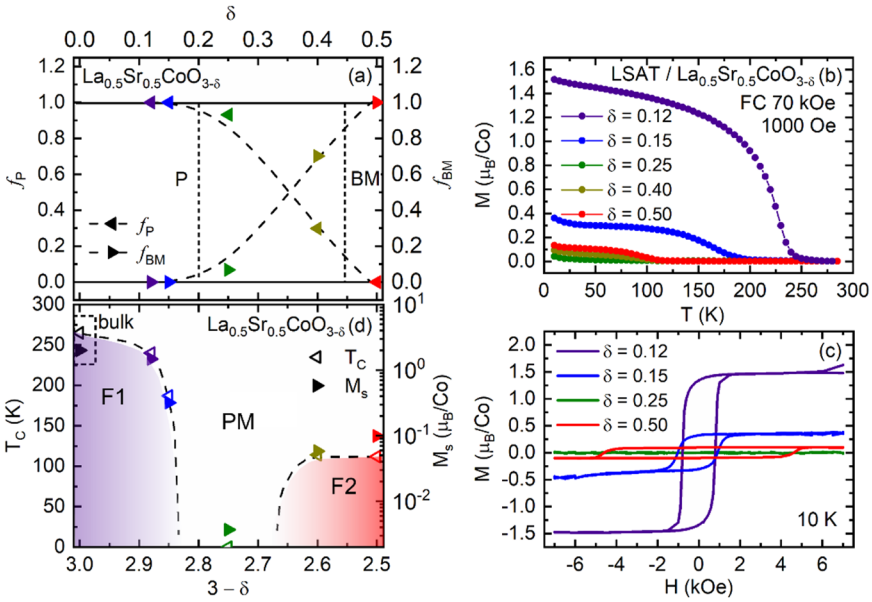

FIG. 4. Magnetic properties of epitaxial $La_{0.5}Sr_{0.5}CoO_{3-\delta}$ thin films as a function of vacuum-annealing-induced δ. (a) Estimated perovskite (P) and brownmillerite (BM) phase fractions (f_P and f_{BM}) from x-ray diffraction peak intensities vs oxygen stoichiometry (3 − δ) (see Fig. S3 of the supplementary material for details). The bottom axis matches with panel (d), and the top axis shows the corresponding estimated δ value [see Figs. 1(f) and S1]. The dashed lines are spline fits. (b) Temperature (T) dependence of the magnetization (M) (in 1000 Oe after field cooling in 70 kOe) of 100-nm-thick $La_{0.5}Sr_{0.5}CoO_{3-\delta}$ films with various δ. (c) 10-K magnetic field (H) dependence of M for the films in (b). The δ = 0.50 film only is at 15 K. (d) Deduced magnetic phase diagram of $La_{0.5}Sr_{0.5}CoO_{3-\delta}$, i.e., magnetic ordering temperature (open points, left axis) vs oxygen stoichiometry (3 − δ). The right axis (solid points) shows the 10-K saturation magnetization on a $\log_{10}$ scale. PM = paramagnetic, and F1 and F2 are the two distinct (P and BM) ferromagnetic phases. The dashed lines are approximate guides to the eye. The black points are bulk data for ~3.0 oxygen stoichiometry, while all the other points are color-coded to match (a)–(c).

T_C drops to ~187 K [Fig. 4(b)], M_s drops to ~0.35 μ_B/Co, and H_c rises slightly to ~1.0 kOe [Fig. 4(c)]. At this stage, the films remain in the phase-pure P state [Fig. 4(a)], with effective doping ($x_{eff} \approx x - 2\delta$ in the simplest model[42,67,78]) of ~0.2. The next largest δ in Figs. 4(a)–4(c) is 0.25 (green), which, according to Fig. 4(a), remains largely in the P phase. The x_{eff} at this point drops to well below the percolation threshold for F metallic behavior ($x \approx 0.18$) in bulk $La_{1-x}Sr_xCoO_3$,[79,80] and, indeed, the F behavior correspondingly vanishes in LSAT/$La_{0.5}Sr_{0.5}CoO_{3-\delta}$. Neither $M(T)$ [Fig. 4(b)] nor $M(H)$ [Fig. 4(c)] suggest any F magnetization in this state. What is remarkable, however, and yet completely consistent with the data of Fig. 3, is that further reduction to $\delta = 0.40$ and 0.50 [where substantial fully ordered BM phase fractions first emerge in Fig. 4(a)—the gold and red points] results in reentrant F behavior. The new F state is characterized by much lower M_s than the P phase [~0.1 μ_B/Co vs ~1.5 μ_B/Co, Fig. 4(c)], lower T_C than the P phase [115 K vs 240 K, Fig. 4(b)], and much larger H_c than the P phase [~46 kOe vs ~1 kOe at 10–15 K, Fig. 4(c)].

The above evolution in magnetic properties is shown in Fig. 4(d), which provides a magnetic phase diagram, complementary to the chemical/structural phase diagram of Fig. 4(a). The right axis of Fig. 4(d) also shows M_s (on a $\log_{10}$ scale) in addition to the T_C on the left axis, and the bulk points are shown for comparison at $\delta \approx 0$. The T_C in the P F phase (open points) is seen to drop precipitously below an oxygen stoichiometry of ~2.85 ($\delta \approx 0.15$), beyond which lies a region of P/BM coexistence [Fig. 4(a)] with no detectable F order [Figs. 4(b)–4(d)]. At oxygen stoichiometry between 2.75 and 2.6 ($\delta \approx 0.35$), reentrant F magnetic order then kicks in [Figs. 4(b)–4(d)], precisely as BM chemical order emerges [Fig. 4(a)]. Notably, the reentrant BM F state of $La_{0.5}Sr_{0.5}CoO_{2.5}$ has distinctly different characteristics to the well-established P F state of $La_{0.5}Sr_{0.5}CoO_3$, specifically $T_C \approx 115$ K, high coercivity, and $M_s \approx 0.1$ μ_B/Co. The latter is reinforced by the solid points in Fig. 4(d) (right axis, on a $\log_{10}$ scale), which highlight the much lower M_s in the BM F state than in the P F state.

As already noted, weak F states are not without precedent in BM-related phases of cobaltites.[4,56,57,81] Nevertheless, the origin of the F state discovered here in BM $La_{0.5}Sr_{0.5}CoO_{2.5}$ is not clear and will undoubtedly require further study for its complete understanding. Significant factors in its origin likely include the existence of both Co^{3+} and Co^{2+} ions ($La_{0.5}Sr_{0.5}CoO_{2.5}$ has an average Co valence of 2.5+ compared to 3+ in $SrCoO_{2.5}$), the complex issue of the spin state of the former, the related issues of the competition between crystal field splitting and Hund exchange, and the nontrivial superexchange pathways in BM phases.[27,47,51,57,66,81] Beneficial future work to further elucidate these issues could be performed with both bulk and thin-film samples, compiling full three-dimensional structural/chemical and magnetic phase diagrams of $La_{1-x}Sr_xCoO_3$ vs x and δ, employing probes such as x-ray spectroscopies and neutron diffraction to fully characterize the nature and origins of the magnetic ordering.

SUMMARY

Stimulated by the growing importance of BM-phase cobaltite thin films in fields such as electrochemical control and magnetoionics, this work provides the first direct neutron-diffraction-based measurement of magnetic order in such materials. BM LSAT/$SrCoO_{2.5}$ films were shown to exhibit G-type AF order but with suppressed $T_N \approx 340$ K. While the origin of the T_N suppression in such films remains to be fully elucidated, this directly confirms bulk-like AF order, opening the door to room-temperature control of antiferromagnetism via electrochemical and thermal redox. Meanwhile, BM LSAT/$La_{0.5}Sr_{0.5}CoO_{2.5}$ films exhibit no such G-type AF order but instead weak F order. The full progression vs δ from $La_{0.5}Sr_{0.5}CoO_3$ to $La_{0.5}Sr_{0.5}CoO_{2.5}$ is found to involve loss of F order as the P phase is reduced, followed by no detectable F order in the P/BM phase coexistence region, and then finally reentrance of a weak F behavior in the BM state. The previously unobserved weak F BM phase of $La_{0.5}Sr_{0.5}CoO_{2.5}$ is characterized by $T_C \approx 115$ K, $M_s \approx 0.1$ μ_B/Co, and strikingly high H_c, quite distinct from the P F phase. While $SrCoO_{3-\delta}$ films thus enable redox toggling between F and AF states (even at room temperature), $La_{0.5}Sr_{0.5}CoO_{3-\delta}$ films therefore enable toggling between F and weak F states. These findings are of interest not only in terms of exploring a new weak F BM phase in the $La_{1-x}Sr_xCoO_{3-\delta}$ system but are also directly relevant to the growing fields of magnetoionics and AF spintronics.

SUPPLEMENTARY MATERIAL

See the supplementary material for Details of lattice mismatches, the estimation of δ from thin-film X-ray diffraction data on $La_{0.5}Sr_{0.5}CoO_{3-\delta}$, powder X-ray diffraction data and cell parameters for bulk BM samples, and further details on the determination of P/BM phase fractions in reduced $La_{0.5}Sr_{0.5}CoO_{3-\delta}$ films.

ACKNOWLEDGMENTS

This work was supported primarily by the National Science Foundation through the University of Minnesota MRSEC under Award No. DMR-2011401. Neutron diffraction was supported by the Department of Energy (DOE) through the University of Minnesota (UMN) Center for Quantum Materials under Grant No. DE-SC0016371. Parts of this work were conducted in the UMN Characterization Facility, which is partially supported by NSF through the MRSEC program under Grant No. DMR-2011401, in the Minnesota Nano Center, which is supported by NSF through the National Nanotechnology Coordinated Infrastructure under Grant No. ECCS2025124, and in the UMN Institute for Rock Magnetism, which is supported by NSF (Earth Sciences Division) under Grant Nos. NSF-EAR 1642268, NSF-EAR 2153786, and by UMN. Parts of this work also used resources at the High Flux Isotope Reactor, a DOE Office of Science User Facility operated by Oak Ridge National Laboratory.

AUTHOR DECLARATIONS

Conflict of Interest

The authors have no conflicts to disclose.

Author Contributions

C.L. and W.M.P. conceived of this study. W.M.P., L.F., and J.L. grew and characterized the films, under the supervision of C.L.

Neutron diffraction measurements and analyses were performed by W.M.P., J.L., N.N., and A.A.A., with input from C.L. This paper was then written by C.L. and W.M.P., with input from all authors.

William M. Postiglione: Conceptualization (supporting); Data curation (lead); Formal analysis (equal); Investigation (lead); Methodology (lead); Writing – original draft (supporting); Writing – review & editing (equal). **Jierui Liang**: Data curation (supporting); Formal analysis (supporting); Investigation (supporting); Methodology (supporting); Writing – review & editing (supporting). **Nileena Nandakumaran**: Data curation (supporting); Formal analysis (supporting); Investigation (supporting); Methodology (supporting); Writing – review & editing (supporting). **Lucca Figari**: Data curation (supporting); Formal analysis (supporting); Investigation (supporting); Methodology (supporting); Writing – review & editing (supporting). **Adam A. Aczel**: Conceptualization (supporting); Data curation (supporting); Formal analysis (supporting); Investigation (supporting); Methodology (supporting); Project administration (supporting); Resources (supporting); Supervision (supporting); Writing – review & editing (supporting). **Chris Leighton**: Conceptualization (lead); Funding acquisition (lead); Project administration (lead); Resources (equal); Supervision (lead); Writing – original draft (lead); Writing – review & editing (equal).

DATA AVAILABILITY

Data supporting the findings of this paper are available either in the paper or supplementary material. Raw data are available from the corresponding author upon reasonable request.

REFERENCES

[1] H. Jeen, W. S. Choi, M. D. Biegalski, C. M. Folkman, I.-C. Tung, D. D. Fong, J. W. Freeland, D. Shin, H. Ohta, M. F. Chisholm, and H. N. Lee, Nat. Mater. **12**, 1057 (2013).

[2] H. Jeen, W. S. Choi, J. W. Freeland, H. Ohta, C. U. Jung, and H. N. Lee, Adv. Mater. **25**, 3651 (2013).

[3] Q. Lu and B. Yildiz, Nano Lett. **16**, 1186 (2016).

[4] N. Lu, P. Zhang, Q. Zhang, R. Qiao, Q. He, H.-B. Li, Y. Wang, J. Guo, D. Zhang, Z. Duan, Z. Li, M. Wang, S. Yang, M. Yan, E. Arenholz, S. Zhou, W. Yang, L. Gu, C.-W. Nan, J. Wu, Y. Tokura, and P. Yu, Nature **546**, 124 (2017).

[5] B. Cui, C. Song, F. Li, X. Y. Zhong, Z. C. Wang, P. Werner, Y. D. Gu, H. Q. Wu, M. S. Saleem, S. S. P. Parkin, and F. Pan, Phys. Rev. Appl. **8**, 044007 (2017).

[6] S. Hu, Y. Wang, C. Cazorla, and J. Seidel, Chem. Mater. **29**, 708 (2017).

[7] B. Cui, P. Werner, T. Ma, X. Zhong, Z. Wang, J. M. Taylor, Y. Zhuang, and S. S. P. Parkin, Nat. Commun. **9**, 3055 (2018).

[8] S. Hu, W. Han, S. Hu, J. Seidel, J. Wang, R. Wu, J. Wang, J. Zhao, Z. Xu, M. Ye, and L. Chen, Chem. Mater. **31**, 6117 (2019).

[9] S. Ning, Q. Zhang, C. Occhialini, R. Comin, X. Zhong, and C. A. Ross, ACS Nano **14**, 8949 (2020).

[10] Q. Lu, S. Huberman, H. Zhang, Q. Song, J. Wang, G. Vardar, A. Hunt, I. Waluyo, G. Chen, and B. Yildiz, Nat. Mater. **19**, 655 (2020).

[11] D. Wang, L. Meng, L. Wei, P. Shi, Y. Chen, S. Yan, Y. Tian, G. Liu, and L. Mei, J. Magn. Magn. Mater. **496**, 165926 (2020).

[12] H. Ji, G. Zhou, X. Wang, J. Zhang, P. Kang, and X. Xu, ACS Appl. Mater. Interfaces **13**, 15774 (2021).

[13] H. Han, A. Sharma, H. L. Meyerheim, J. Yoon, H. Deniz, K.-R. Jeon, A. K. Sharma, K. Mohseni, C. Guillemard, M. Valvidares, P. Gargiani, and S. S. P. Parkin, ACS Nano **16**, 6206 (2022).

[14] Q. Zhang, G. Hu, V. Starchenko, G. Wan, E. M. Dufresne, Y. Dong, H. Liu, H. Zhou, H. Jeen, K. Saritas, J. T. Krogel, F. A. Reboredo, H. N. Lee, A. R. Sandy, I. C. Almazan, P. Ganesh, and D. D. Fong, Phys. Rev. Lett. **129**, 235701 (2022).

[15] A. Khare, D. Shin, T. S. Yoo, M. Kim, T. D. Kang, J. Lee, S. Roh, I.-H. Jung, J. Hwang, S. W. Kim, T. W. Noh, H. Ohta, and W. S. Choi, Adv. Mater. **29**, 1606566 (2017).

[16] M. S. Saleem, B. Cui, C. Song, Y. Sun, Y. Gu, R. Zhang, M. U. Fayaz, X. Zhou, P. Werner, S. S. P. Parkin, and F. Pan, ACS Appl. Mater. Interfaces **11**, 6581 (2019).

[17] B. M. Lefler, T. Duchoň, G. Karapetrov, J. Wang, C. M. Schneider, and S. J. May, Phys. Rev. Mater. **3**, 073802 (2019).

[18] L. Wang, Y. Du, L. Chang, K. A. Stoerzinger *et al.*, Appl. Phys. Lett. **114**, 231602 (2019).

[19] B. M. Lefler, W. M. Postiglione, C. Leighton, and S. J. May, Adv. Funct. Mater. **32**, 2208434 (2022).

[20] Y. Xing, I. Kim, K. T. Kang, B. Park, Z. Wang, J. Chan Kim, H. Y. Jeong, W. S. Choi, J. Lee, and S. H. Oh, Matter **5**, 3009 (2022).

[21] Y. Takeda, R. Kanno, T. Takada, O. Yamamoto, M. Takano, and Y. Bando, Z. Anorg. Allg. Chem. **540**, 259 (1986).

[22] A. Nemudry, P. Rudolf, and R. Schöllhorn, Chem. Mater. **8**, 2232 (1996).

[23] J. P. Hodges, S. Short, J. D. Jorgensen, X. Xiong, B. Dabrowski, S. M. Mini, and C. W. Kimball, J. Solid State Chem. **151**, 190 (2000).

[24] S. Stemmer, A. Sane, N. D. Browning, and T. J. Mazanec, Solid State Ionics **130**, 71 (2000).

[25] Y. Ito, R. F. Klie, N. D. Browning, and T. J. Mazanec, J. Am. Ceram. Soc. **85**, 969 (2004).

[26] R. Le Toquin, W. Paulus, A. Cousson, C. Prestipino, and C. Lamberti, J. Am. Chem. Soc. **128**, 13161 (2006).

[27] A. Muñoz, C. de la Calle, J. A. Alonso, P. M. Botta, V. Pardo, D. Baldomir, and J. Rivas, Phys. Rev. B **78**, 054404 (2008).

[28] L. Karvonen, H. Yamauchi, and M. Karppinen, Chem. Mater. **20**, 7143 (2008).

[29] L. Karvonen, S. Yoon, P. Hug, H. Yamauchi, A. Weidenkaff, and M. Karppinen, Mater. Res. Bull. **46**, 1340 (2011).

[30] C. K. Xie, Y. F. Nie, B. O. Wells, J. I. Budnick, W. A. Hines, and B. Dabrowski, Appl. Phys. Lett. **99**, 052503 (2011).

[31] J. Young and J. M. Rondinelli, Phys. Rev. B **92**, 174111 (2015).

[32] C. Leighton, Nat. Mater. **18**, 13 (2019).

[33] C. Navarro-Senent, A. Quintana, E. Menéndez, E. Pellicer, and J. Sort, APL Mater. **7**, 030701 (2019).

[34] A. Molinari, H. Hahn, and R. Kruk, Adv. Mater. **31**, 1806662 (2019).

[35] M. Nichterwitz, S. Honnali, M. Kutuzau, S. Guo, J. Zehner, K. Nielsch, and K. Leistner, APL Mater. **9**, 030903 (2021).

[36] Y. Guan, H. Han, F. Li, G. Li, and S. S. P. Parkin, Annu. Rev. Mater. Res. **53**, 25 (2023).

[37] F. R. Van Buren, G. H. J. Broers, A. J. Bouman, and C. Boesveld, J. Electroanal. Chem. Interfacial Electrochem. **88**, 353 (1978).

[38] A. Nemudry, E. L. Goldberg, M. Aguirre, and M. Á. Alario-Franco, Solid State Sci. **4**, 677 (2002).

[39] J. T. Mefford, X. Rong, A. M. Abakumov, W. G. Hardin, S. Dai, A. M. Kolpak, K. P. Johnston, and K. J. Stevenson, Nat. Commun. **7**, 11053 (2016).

[40] H. A. Tahini, X. Tan, U. Schwingenschlögl, and S. C. Smith, ACS Catal. **6**, 5565 (2016).

[41] A. Grimaud, O. Diaz-Morales, B. Han, W. T. Hong, Y.-L. Lee, L. Giordano, K. A. Stoerzinger, M. T. M. Koper, and Y. Shao-Horn, Nat. Chem. **9**, 457 (2017).

[42] V. Chaturvedi, W. M. Postiglione, R. D. Chakraborty, B. Yu, W. Tabiś, S. Hameed, N. Biniskos, A. Jacobson, Z. Zhang, H. Zhou, M. Greven, V. E. Ferry, and C. Leighton, ACS Appl. Mater. Interfaces **13**, 51205 (2021).

[43] W. M. Postiglione, G. Yu, V. Chaturvedi, H. Zhou, K. Heltemes, A. Jacobson, M. Greven, and C. Leighton, "Mechanisms of hysteresis and reversibility across the voltage-driven Perovskite-Brownmillerite transformation in electrolyte-gated ultrathin $La_{0.5}Sr_{0.5}CoO_{3-\delta}$," (published online, 2024).

[44] Y. Long, Y. Kaneko, S. Ishiwata, Y. Taguchi, and Y. Tokura, J. Phys. Condens. Matter **23**, 245601 (2011).

[45] S. Kawasaki, M. Takano, and Y. Takeda, J. Solid State Chem. **121**, 174 (1996).

[46]P. Bezdicka, A. Wattiaux, J. C. Grenier, M. Pouchard, and P. Hagenmuller, Z. Anorg. Allg. Chem. **619**, 7 (1993).
[47]T. Takeda, Y. Yamaguchi, and H. Watanabe, J. Phys. Soc. Jpn. **33**, 970 (1972).
[48]J. Rodriguez, J. M. Gonzalez-Calbet, J. C. Grenier, J. Pannetier, and M. Anne, Solid State Commun. **62**, 231 (1987).
[49]F. Hong, B. Yue, Z. Liu, B. Chen, and H.-K. Mao, Phys. Rev. B **95**, 024115 (2017).
[50]B. C. Behera, S. Jana, S. G. Bhat, N. Gauquelin, G. Tripathy, P. S. Anil Kumar, and D. Samal, Phys. Rev. B **99**, 024425 (2019).
[51]S. Chowdhury, A. Jana, M. Kuila, V. R. Reddy, R. J. Choudhary, and D. M. Phase, ACS Appl. Electron. Mater. **2**, 3859 (2020).
[52]S. J. Callori, S. Hu, J. Bertinshaw, Z. J. Yue, S. Danilkin, X. L. Wang, V. Nagarajan, F. Klose, J. Seidel, and C. Ulrich, Phys. Rev. B **91**, 140405 (2015).
[53]T. Jungwirth, X. Marti, P. Wadley, and J. Wunderlich, Nat. Nanotechnol. **11**, 231 (2016).
[54]V. Baltz, A. Manchon, M. Tsoi, T. Moriyama, T. Ono, and Y. Tserkovnyak, Rev. Mod. Phys. **90**, 015005 (2018).
[55]H. Huang, J. Zhang, H. Zhang, F. Han, X. Chen, J. Song, J. Zhang, S. Qi, Y. Chen, J. Cai, F. Hu, B. Shen, and J. Sun, J. Phys. D: Appl. Phys. **53**, 155003 (2020).
[56]I.-T. Chiu, M.-H. Lee, S. Cheng, S. Zhang, L. Heki, Z. Zhang, Y. Mohtashami, P. N. Lapa, M. Feng, P. Shafer, A. T. N'Diaye, A. Mehta, J. A. Schuller, G. Galli, S. Ramanathan, Y. Zhu, I. K. Schuller, and Y. Takamura, Phys. Rev. Mater. **5**, 064416 (2021).
[57]Q. Zhang, A. Gao, F. Meng, Q. Jin, S. Lin, X. Wang, D. Xiao, C. Wang, K.-J. Jin, D. Su, E.-J. Guo, and L. Gu, Nat. Commun. **12**, 1853 (2021).
[58]S. Zhang, I.-T. Chiu, M.-H. Lee, B. Gunn, M. Feng, T. J. Park, P. Shafer, A. T. N'Diaye, F. Rodolakis, S. Ramanathan, A. Fraño, I. K. Schuller, Y. Takamura, and G. Galli, Chem. Mater. **34**, 2076 (2022).
[59]D. A. Gilbert, A. J. Grutter, P. D. Murray, R. V. Chopdekar, A. M. Kane, A. L. Ionin, M. S. Lee, S. R. Spurgeon, B. J. Kirby, B. B. Maranville, A. T. N'Diaye, A. Mehta, E. Arenholz, K. Liu, Y. Takamura, and J. A. Borchers, Phys. Rev. Mater. **2**, 104402 (2018).
[60]G. Rippy, L. Trinh, A. M. Kane, A. L. Ionin, M. S. Lee, R. V. Chopdekar, J. M. Christiansen-Salameh, D. A. Gilbert, A. J. Grutter, P. D. Murray, M. V. Holt, Z. Cai, K. Liu, Y. Takamura, and R. Kukreja, Phys. Rev. Mater. **3**, 082001 (2019).
[61]J. Walter, G. Yu, B. Yu, A. Grutter, B. J. Kirby, J. Borchers, Z. Zhang, H. Zhou, T. Birol, M. Greven, and C. Leighton, Phys. Rev. Mater. **1**, 071403(R) (2017).
[62]J. Song, Y. Chen, X. Chen, T. Khan, F. Han, J. Zhang, H. Huang, H. Zhang, W. Shi, S. Qi, F. Hu, B. Shen, and J. Sun, Phys. Rev. Appl. **14**, 024062 (2020).
[63]Y. Zhang, W. M. Postiglione, R. Xie, C. Zhang, H. Zhou, V. Chaturvedi, K. Heltemes, H. Zhou, T. Feng, C. Leighton, and X. Wang, Nat. Commun. **14**, 2626 (2023).
[64]R. D. Chakraborty, W. M. Postiglione, S. Ghosh, K. A. Mkhoyan, C. Leighton, and V. E. Ferry, Adv. Opt. Mater. **11**, 2300098 (2023).
[65]Z. Yin, J. Wang, J. Wang, J. Li, H. Zhou, C. Zhang, H. Zhang, J. Zhang, F. Shen, J. Hao, Z. Yu, Y. Gao, Y. Wang, Y. Chen, J.-R. Sun, X. Bai, J.-T. Wang, F. Hu, T.-Y. Zhao, and B. Shen, ACS Nano **16**, 14632 (2022).
[66]S. Kolesnik, B. Dabrowski, J. Mais, M. Majjiga, O. Chmaissem, A. Baszczuk, and J. D. Jorgensen, Phys. Rev. B **73**, 214440 (2006).
[67]J. Walter, T. Charlton, H. Ambaye, M. R. Fitzsimmons, P. P. Orth, R. M. Fernandes, and C. Leighton, Phys. Rev. Mater. **2**, 111406(R) (2018).
[68]J. Ovenstone, J. S. White, and S. T. Misture, J. Power Sources **181**, 56 (2008).
[69]Y.-M. Kim, J. He, M. D. Biegalski, H. Ambaye, V. Lauter, H. M. Christen, S. T. Pantelides, S. J. Pennycook, S. V. Kalinin, and A. Y. Borisevich, Nat. Mater. **11**, 888 (2012).
[70]S. Inkinen, L. Yao, and S. van Dijken, Phys. Rev. Mater. **4**, 046002 (2020).
[71]B. C. Chakoumakos, D. G. Schlom, M. Urbanik, and J. Luine, J. Appl. Phys. **83**, 1979 (1998).
[72]R. C. O'Handley, *Modern Magnetic Materials Principles and Applications* (John Wiley & Sons, New York, 2000).
[73]J. Tuček, R. Zbořil, A. Namai, and S. Ohkoshi, Chem. Mater. **22**, 6483 (2010).
[74]M. Shang, C. Zhang, T. Zhang, L. Yuan, L. Ge, H. Yuan, and S. Feng, Appl. Phys. Lett. **102**, 062903 (2013).
[75]B. D. Cullity and C. D. Graham, *Introduction to Magnetic Materials*, 2nd ed. (John Wiley & Sons, Hoboken, NJ, 2009).
[76]M. Huang, M. U. Hasan, K. Klyukin, D. Zhang, D. Lyu, P. Gargiani, M. Valvidares, S. Sheffels, A. Churikova, F. Büttner, J. Zehner, L. Caretta, K.-Y. Lee, J. Chang, J.-P. Wang, K. Leistner, B. Yildiz, and G. S. D. Beach, Nat. Nanotechnol. **16**, 981 (2021).
[77]S. Zhang and G. Galli, "Electronic Properties of the interface between Perovskite and brownmillerite Phases in $La_{1-x}Sr_xCo_{3-\delta}$," in American Physical Society, APS March Meeting, 2023.
[78]M. A. Torija, M. Sharma, J. Gazquez, M. Varela, C. He, J. Schmitt, J. A. Borchers, M. Laver, S. El-Khatib, and C. Leighton, Adv. Mater. **23**, 2711 (2011).
[79]J. Wu and C. Leighton, Phys. Rev. B **67**, 174408 (2003).
[80]H. M. Aarbogh, J. Wu, L. Wang, H. Zheng, J. F. Mitchell, and C. Leighton, Phys. Rev. B **74**, 134408 (2006).
[81]H. Li, F. Lou, Y. Wang, Y. Zhang, Q. Zhang, D. Wu, Z. Li, M. Wang, T. Huang, Y. Lyu, J. Guo, T. Chen, Y. Wu, E. Arenholz, N. Lu, N. Wang, Q. He, L. Gu, J. Zhu, C.-W. Nan, X. Zhong, H. Xiang, and P. Yu, Adv. Sci. **6**, 1901432 (2019).